A Moving Mesh Approach to a Shallow Ice Glacier Model incorporating Data Assimilation

D. Partridge   M.J. Baines,

N.K. Nichols

Department of Mathematics and Statistics,

University of Reading, UK

March 2014

Abstract

We present a conservation-based moving point method and some data assimilation experiments using the method, applied to a simplified shallow ice model with a moving boundary that incorporates ice diffusion and net ice-equivalent accumulation/ablation.

We assess the behaviour of the diffusive velocity in the vicinity of the moving boundary and determine criteria upon the local profile under which the glacier front will advance or remain stationary.

A conservation-based description of the flow is then introduced which determines a deformation velocity that is used to define the movement of the glacier in the presence of both ice diffusion and accumulation.

A finite difference approximation based on the conservation description is applied and tested using a simple test scenario to reproduce different types of glacier flow. Comparisons are drawn with some existing non-moving mesh solutions and exact solutions to one of the European Ice Sheet Modelling INiTiative (EISMINT) test problems.

Techniques for data assimilation within the moving framework are then presented and used to incorporate sparsely measured observations of the ice sheet profile into the computational model, resulting in better forecasts of the ice flow.

---

1   Introduction

Much work in cryospheric simulation is devoted to increasing the accuracy of mathematical models to reduce the uncertainty in estimates of the flow of glaciers and ice sheets in order to provide better predictions for the future. It is only relatively recently that dynamical ice flow models have started to be included within global climate models, part of the reason being the large degree of uncertainty associated with the models, whilst computational expense is another key factor. Dynamical ice flow models require a higher resolution than is currently present in climate models: an alternative to increasing the resolution

everywhere is to apply adaptive mesh techniques which allows improved approximations to be made in key areas. A number of current simulations utilise mesh refinement to increase the resolution in certain chosen areas, which works well provided the domain is reasonably well understood and the areas that require higher resolution can be approximately identified and are slowly varying. Another approach is to move the computational mesh nodes to required areas which has been shown to be more robust than non-adaptive methods, [9]: these methods move the nodes at fixed times and are typically controlled by a monitor function which can however be awkward to define, [3]. In other fields the movement of the mesh nodes is defined in terms of a time-dependent velocity, which introduces a more intuitive definition of the monitor function and allows the mesh to be influenced by its previous position, [1, 2]. Currently this approach has not been applied to the dynamical ice flow equations, an issue that is addressed in this paper.

2   Shallow Ice Approximation

Under the shallow ice assumptions for glaciers and ice sheets the ice thickness satisfies a single partial differential equation (PDE) arising from mass balance. To derive this equation it is assumed that the depth of the ice is shallow in comparison to the horizontal extent, meaning that vertical shear stresses can be excluded [6]. The flow of ice follows a constitutive relationship (e.g. the Glen-Nye flow law, [5]) while variations in the temperature and density of the ice are ignored.

The one-dimensional model follows a flowline of the glacier. The shallow ice equation then takes the form

$$\frac{\partial h}{\partial t} + \frac{\partial (hu)}{\partial x} = m(x) \tag{1}$$

in the moving domain $(0 < x < b(t))$, where $h(x,t)$ is the depth-averaged ice thickness and $m(x)$ the ice-equivalent accumulation rate (which includes the effect of ablation). In eq. (1) $u(x,t)$ is the flow velocity due to ice diffusion which

is described in detail in Section 3 below. There are two boundary conditions:
a no-flux condition at the ice divide (at $x = 0$) and zero ice thickness at the
moving front, i.e.

$$\frac{\partial h}{\partial x} = 0 \quad \text{at } x = 0, \qquad h = 0 \quad \text{at } x = b(t). \tag{2}$$

The total ice in the whole domain, denoted here by $\theta(t)$, is defined as

$$\int_0^{b(t)} h(x,t)dx = \theta(t), \tag{3}$$

and has the following property, to be referred to later. Differentiating eq. (3)
with respect to t using Leibnitz' integral rule gives

$$\dot{\theta} = \frac{d}{dt} \int_0^{b(t)} h(x,t)dx \tag{4}$$

$$= \int_0^{b(t)} \frac{\partial h}{\partial t} dx + h(b,t) \frac{db}{dt} \tag{5}$$

Since $h = 0$ at $x = b(t)$ the second term is zero. Substituting eq. (1) into eq. (5)
results in

$$\dot{\theta} = - \int_0^{b(t)} \frac{\partial(hu)}{\partial x} dx + \int_0^{b(t)} m(x)dx \tag{6}$$

$$= -hu \Big|_{x=0}^{b(t)} + \int_0^{b(t)} m(x)dx$$

Use of the boundary conditions, eq. (2), again forces the first term to be zero,
since the ice flow is zero at the ice divide. This leaves the rate of change of the
total ice over the domain as

$$\dot{\theta} = \int_0^{b(t)} m(x)dx. \tag{7}$$

As a result any change in the total ice over the whole glacier is due solely to the
source term in eq. (7), i.e. the rate of change of global ice thickness equates to
the net accumulation/ablation over the whole glacier.

3 Diffusive Velocity at the Glacier Front

The diffusive flow velocity of glaciers ($u(x,t)$ in eq. (1)) is typically dominated
by the underlying topography and the surface elevation. In this section the

movement of the glacier front generated by this diffusive flow velocity is assessed.

Under the shallow ice approximation the diffusive velocity $u(x,t)$ in eq. (1) can be written as

$$u(x,t) = c\{h(x,t)\}^{n+1} s_x^n, \tag{8}$$

(see e.g. [9]) under the assumption that temperature and density remain constant throughout the glacier, where c is a negative constant. The surface elevation $s(x)$ is the glacier height comprising the topographical bed and ice thickness.

3.1 Without topography

Upon the assumption that the bed is flat eq. (8) becomes

$$u(x,t) = c\{h(x,t)\}^{n+1}\{h_x\}^n. \tag{9}$$

The form of eq. (9) suggests a difficulty when applying the boundary condition $h = 0$ at $x = b(t)$, apparently yielding a zero diffusive velocity and resulting in a boundary that only moves as a result of accumulation or ablation. However, it is perfectly possible for the diffusive velocity u to be non-zero when $h(b,t) = 0$ provided that $h_x(b.t)$ is infinite such that $\{h(b,t)\}^{n+1}\{h_x(b,t)\}^n$ is finite. Using the chain rule for differentiation and writing eq. (9) in the more useful form

$$u = c\{h(x,t)\}^{(n+1)/n}(h_x)^n = c\left(\frac{n}{2n+1}\right)^n\left\{\left(\{h(x,t)\}^{(2n+1)/n}\right)_x\right\}^n, \tag{10}$$

it can be seen that the diffusive velocity is finite at the boundary provided that $\{\{h(x.t)\}^{(2n+1)/n}\}_x$ is finite there.

The local behaviour of eq. (9) at the moving boundary can be analysed further. Suppose that $b(t) = b$ is fixed. Due to the boundary condition $h = 0$ at $x = b$ the ice thickness profile $h(b,x)$ contains a positive power of $(b-x)$. Let $\alpha > 0$ be the largest real number such that $h(x,t)$ can be written in the form

$$h(x,t) = (b-x)^\alpha g(x,t) \tag{11}$$

where the function $g(x,t) > 0$ is finite and has a finite x derivative at the boundary $x = b$. Then

$$\{h(x,t)\}^{(2n+1)/n} = \{(b-x)^\alpha g(x,t)\}^{(2n+1)/n} = (b-x)^{\alpha(2n+1)/n} G(x,t), \quad (12)$$

where $G(x,t) = g(x,t)^{(2n+1)/n} > 0$ also has a finite x derivative at $x = b$. The value of $u(x,t)$ at the boundary is proportional to the derivative of the left hand side of eq. (12) and thus proportional to the limit of eq. (10) as x tends to b, i.e.

$$\lim_{x\to b}(\{h(x,t)\}^{(2n+1)/n})_x = -\lim_{x\to b}\frac{(b-x)^{\alpha(2n+1)/n}G(x,t)}{(b-x)}$$

$$= -\lim_{x\to b}(b-x)^{(\alpha(2n+1)/n)-1}G(x,t),$$

using l'Hopital's rule. It follows that the limit of the diffusive velocity (eq. (10)) is proportional to

$$\lim_{x\to b}(b-x)^{\alpha(2n+1)-n}. \quad (13)$$

Since n is a given exponent, there exists a critical value for the power α, denoted α_c, which leads to the following behaviour of the diffusive velocity $u(x,t)$ at the boundary as $x \to b$:

$$\text{Case 1:} \quad \alpha \; > \; \alpha_c \quad \Rightarrow \quad u \to 0 \text{ as } x \to b\,, \quad (14)$$

$$\text{Case 2:} \quad \alpha \; = \; \alpha_c \quad \Rightarrow \quad u \text{ remains finite as } x \to b\,, \quad (15)$$

$$\text{Case 3:} \quad \alpha \; < \; \alpha_c \quad \Rightarrow \quad u \to \infty \text{ as } x \to b \text{ (momentarily)}\,. \quad (16)$$

where the critical value of α is given by

$$\alpha_c = \frac{n}{(2n+1)}. \quad (17)$$

Thus the diffusive velocity $u(x,t)$ induces no movement at the boundary when the value of α in the ice thickness profile given in eq. (11) lies in the range $\alpha > \alpha_c = n/(2n+1)$. However, as the ice thickness profile changes over time such that α tends to the critical value α_c of eq. (17), the condition in Case 2 is met and the diffusive velocity becomes non-zero. If the thickness profile reaches the condition of Case 3 then the velocity is unbounded, at least momentarily.

Taking the standard value used in ice sheet modelling, $n = 3$, eq. (17) gives

6
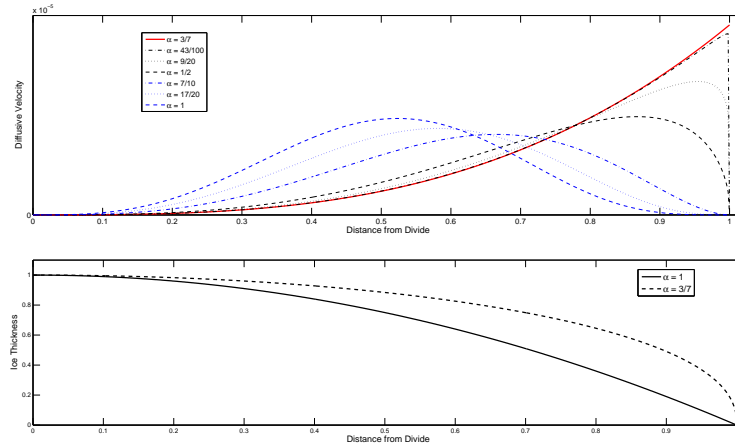
Figure 1: (a) Diffusive velocity. When $\alpha = 3/7$ (red line) the boundary velocity is finite whereas all other values have a zero boundary velocity. (b) Ice thickness profiles for $\alpha = 1$ (solid) and $\alpha = 3/7$ (dashed). Notice the infinite gradient at the boundary when $\alpha \to 3/7$.

the critical value as $\alpha_c = 3/7$. As a demonstration suppose that the initial thickness profile takes the form

$$h(x,t) = (b-x)^\alpha (b+x)^\alpha \tag{18}$$

with the boundary at $b = 1$. By varying the value of α the diffusive velocity at the boundary changes discontinuously from zero to a finite value at the momennt that α reaches $3/7$ from above (see fig. 1a)). In Figure 1b) it can be seen that when α reaches the critical value the gradient of the ice at the boundary becomes infinite, which was identified in eq. (9) as a sufficient condition for a non-zero velocity.

Because the gradient at the boundary increases in modulus under ice movement the value of α decreases from a value of order 1 towards $\alpha \to 3/7$ from above as the peak velocity approaches the boundary.

7

3.2 Introducing topography

Removing the assumption that the bed of the glacier is flat, the surface elevation is a summation of the bed and ice components

$$s(x,t) = z(x) + h(x,t), \tag{19}$$

where $z(x)$ represents the topography under the glacier. With $n = 3$ the diffusive velocity in eq. (8) may then be written as

$$u(x,t) = c\{h(x,t)\}^4 \left(\{z(x) + h(x,t)\}_x\right)^3 \tag{20}$$

$$= cz_x^3\{h(x,t)\}^4 + 3cz_x^2\{h(x,t)\}^4 h_x + 3cz_x\{h(x,t)\}^4 h_x^2 + c\{h(x,t)\}^4 h_x^3. \tag{21}$$

The last term in eq. (21) is the same as the single term in the flat bed scenario, eq. (9) with $n = 3$. Expressing the terms in eq. (21) in the form used in eq. (10) gives

$$u(x,t) = c\,(z_x)\{h(x,t)\}^4 + \frac{3c}{5}(z_x)^2\left(\{h(x,t)\}^5\right)_x + \frac{c}{3}z_x\left\{\left(\{h(x,t)\}^3\right)_x\right\}^2$$
$$+ \frac{9c}{343}\left\{\left(\{h(x,t)\}^{7/3}\right)_x\right\}^3. \tag{22}$$

Substituting for h from eq. (11),

$$u(x,t) = c\,(z_x)^3(b-x)^{4\alpha}\{g(x,t)\}^4 + \frac{3c}{5}(z_x)^2\left\{(b-x)^{5\alpha}\{g(x,t)\}^5\right\}_x$$
$$+ \frac{c}{3}z_x\left(\left\{(b-x)^{3\alpha}\{g(x,t)\}^3\right\}_x\right)^2 + \frac{9c}{343}\left(\left\{(b-x)^{7\alpha/3}\{g(x)\}^{7/3}\right\}_x\right)^3. \tag{23}$$

At the moving boundary the diffusive velocity can be found by taking the limit of $u(x,t)$ as $x \to b$, i.e. from eq. (23)

$$\lim_{x \to b} u(x,t) = \lim_{x \to b}\left[c\,(z_x)^3(b-x)^{4\alpha}\{g(x,t)\}^4 + \frac{3c}{5}(z_x)^2\left\{(b-x)^{5\alpha}\{g(x,t)\}^5\right\}_x\right.$$
$$\left. + \frac{c}{3}z_x\left(\left\{(b-x)^{3\alpha}\{g(x,t)\}^3\right\}_x\right)^2 + \frac{9c}{343}\left(\left\{(b-x)^{7\alpha/3}g(x,t)^{7/3}\right\}_x\right)^3\right]. \tag{24}$$

The first term tends to zero at the boundary and, applying L'Hopital's rule to

the remaining three terms individually, leaves

$$u(b,t) = -\frac{3c}{5}(z_b)^2 \lim_{x\to b}\left\{(b-x)^{5\alpha-1}\{g(x)\}^5\right\}$$
$$+ \frac{c}{3}z_b\left(-\lim_{x\to b}\{(b-x)^{3\alpha-1}\{g(x,t)\}^3\}\right)^2$$
$$+ \frac{9c}{343}\left(-\lim_{x\to b}\left(\{(b-x)^{7\alpha/3-1}\{g(x,t)\}^{7/3}\}\right)\right)^3. \quad (25)$$

Each term separately yields a different critical value of α, namely $\alpha_c = 1/5, 1/3$ and $3/7$ for each term respectively. However, since α cannot go below any of these values without encountering an infinite velocity (see section 3.1), the lower limit for α must be the largest value, namely $3/7$. Therefore the flat bed analysis holds with the same conditions on the diffusive velocity at the boundary in section 3.1, regardless of whether there is a topographic bed present.

In the absence of accumulation/ablation this is the sole cause of ice movement at the boundary, which allows the determination of when the glacier remains stationary and when boundary movement will commence.

Of course, varying the temperature and density will result in a different value for the finite velocity achieved when the condition of Case 2 is met. Nevertheless, the boundary velocity will remain zero when α lies in the Case 1 range regardless of the temperature or density.

4 Conservation of Mass Fractions (CMF)

We now develop a description of glacier movement using a moving spatial coordinate by determining a velocity based upon both ice diffusion and accumulation/ablation, utilising an approach found in [1, 2].

Let $\widehat{x}(x,t)$ be a moving point that coincides with the x coordinate at time t and define the relative mass in the moving interval $(0, \widehat{x}(t))$ as

$$\frac{1}{\theta(t)}\int_0^{\widehat{x}(t)} h(x,t)dx \quad (26)$$

where $\theta(t)$ is the total ice mass, given in (7). The time rate of change of $\widehat{x}(t)$ is

derived implicitly by enforcing the assumption of partial relative conservation,

$$\frac{1}{\theta(t)} \int_0^{\widehat{x}(t)} h(x,t)dx = \mu(\widehat{x}), \tag{27}$$

where $\mu(\widehat{x})$ is independent of time for all moving subdomains of $[0, b(t)]$. Note that $\mu(\widehat{x}) \in [0,1]$ is a cumulative function with $\mu(0) = 0$ and $\mu(b) = 1$.

4.1 The Deformation Velocity

To extract the velocity $d\widehat{x}/dt$ differentiate (27) with respect to time,

$$\frac{d}{dt} \int_0^{\widehat{x}(t)} h(x,t)dx = \mu(\widehat{x})\dot{\theta} \tag{28}$$

Carrying out the time differentiation using Leibnitz' Integral Rule and substituting for h_t from eq. (1) gives

$$
\begin{aligned}
\frac{d}{dt} \int_0^{\widehat{x}(t)} h(x,t)dx &= \int_0^{\widehat{x}(t)} h_t dx + \left. \left(h \frac{dx}{dt} \right) \right|_0^{\widehat{x}(t)} \\
&= \int_0^{\widehat{x}(t)} \{-(hu)_x + m(x)\} \, dx + h(\widehat{x}, t) \frac{d\widehat{x}}{dt} \\
&= \int_0^{\widehat{x}(t)} m(x)dx + \left(-h(\widehat{x},t)u(\widehat{x},t) + h(\widehat{x},t)\frac{d\widehat{x}}{dt} \right) \tag{29}
\end{aligned}
$$

since $d\widehat{x}/dt$ vanishes at the fixed boundary $x = 0$. From eq. (28), eq. (29) and eq. (7) the deformation velocity at an arbitrary interior point is then

$$\frac{d\widehat{x}}{dt} = u + \frac{\left[\mu(\widehat{x}) \int_0^{b(t)} m(x)dx - \int_0^{\widehat{x}(t)} m(x)dx \right]}{h}. \tag{30}$$

Equation eq. (30) determines the net overall movement of the point $\widehat{x}$ in the glacial domain as a combination of the flow velocity $u(x,t)$ and the accumulation rate $m(x)$.

4.2 The Net Velocity at the Glacier Front

The net velocity at the moving front at $x = b(t)$ may be found by taking the limit of eq. (30) as $\widehat{x}(t) \to b(t)$, i.e.

$$\lim_{\widehat{x}(t) \to b(t)} \frac{d\widehat{x}}{dt} = u(\widehat{x},t)|_{b(t)} + \lim_{\widehat{x}(t) \to b} \frac{1}{h(\widehat{x},t)} \left[\mu \int_0^{b(t)} m(x)dx - \int_0^{\widehat{x}(t)} m(x)dx \right]. \tag{31}$$

10

Since $h \to 0$ the limit in eq. (31) as $\widehat{x} \to b$ is undefined. Nevertheless, since the quantity in square brackets also $\to 0$ as $\widehat{x}(t) \to b$, then assuming continuity of $\frac{d\widehat{x}}{dt}$ and $m(x)$ in the vicinity of the boundary, by l'Hopital's Rule

$$\lim_{\widehat{x}(t) \to b(t)} \frac{d\widehat{x}}{dt} = u(b(t), t) + \lim_{\widehat{x}(t) \to b(t)} \left\{ \frac{\frac{d}{d\widehat{x}} \left(\mu \int_0^{b(t)} m(x)dx - \int_0^{\widehat{x}(t)} m(x)dx \right)}{h_x} \right\}$$

$$= u(b(t), t) - \frac{m(b(t))}{h_x(b(t), t)} \tag{32}$$

The boundary velocity generated in this way incorporates both the ice-equivalent accumulation $m(b(t))$ and the diffusive velocity $u(b(t), t)$ at the moving boundary. Since $h_x < 0$ at the front the second term in eq. (32) is positive or negative depending on whether $m(b(t))$ is positive or negative. If the gradient h_x at the front is shallow the net boundary velocity is dominated by the accumulation/ablation component of eq. (32), allowing the front to advance or retreat. Conversely, if the gradient h_x at the front is steep, the flow velocity u dominates. The front is then susceptible to the analysis of the diffusive velocity in section 3, and the boundary of the glacier can therefore only advance or wait, not retreat.

4.3 Movement of the Glacial Domain

Once the velocities $d\widehat{x}/dt$ of the points $\widehat{x}(x, t)$ of the glacial domain have been found from eq. (30) they can be moved accordingly. In addition the increase or decrease in the total ice $\theta(t)$ can be determined from eq. (7).

4.4 The Ice Thickness Profile

After updating $\widehat{x}(x, t)$ and $\theta(t)$ the ice thickness profile is deduced from eq. (27)). Differentiating with respect to $\widehat{x}$,

$$h(\widehat{x}, t) = \theta(t) \frac{\partial \mu(\widehat{x})}{\partial \widehat{x}}, \tag{33}$$

which allows the ice thickness profile to be constructed.

5 A finite-difference algorithm

The velocity-based conservation description of the previous section is now discretised using finite differences on an irregularly moving mesh $\{X_i\}$, $(i = 1, 2, ..., N)$, where

$$0 = X_1(t) < X_2(t) < \cdots < X_N(t) = b(t) \tag{34}$$

The approximation of $h(x,t)$ at $X = X_i$ is written as H_i and that of the diffusive velocity $u(x,t)$ as U_i.

It is convenient to split the numerical scheme into three stages which are repeated at each time step. Stage 1 of the algorithm is to approximate equation eq. (30) to give a discrete velocity at each interior node of the form

$$\frac{dX_i}{dt} = U_i + \frac{\left\{ \mu_i \int_0^{b(t)} m(x)dx - \int_0^{X_i(t)} m(x)dx \right\}}{H_i}, \tag{35}$$

where μ_i denotes $\mu(X_i)$ and where U_i is approximated from (10) in an upwind manner as

$$U_i = c \left(\frac{n}{2n+1} \right)^n \left\{ \frac{\{H_i\}^{(2n+1)/n} - \{H_{i-1}\}^{(2n+1)/n}}{X_i - X_{i-1}} \right\}^n \tag{36}$$

The integrals in (35) are approximated by a composite trapezium rule.

In the second stage the X_i are advanced in time using the explicit Euler scheme, i.e.

$$X_i^{k+1} = X_i^k + \Delta t \left(\frac{dX_i}{dt} \right)^k. \tag{37}$$

for all i, where k denotes the time discretisation level. Explicit Euler time-stepping is adequate for our purpose provided that the time step is sufficiently small to prevent node-overtaking. The explicit Euler time stepping scheme is also used to update the total mass θ^{k+1} from eq. (7), i.e.

$$\theta^{k+1} = \theta^k + \Delta t \int_0^{b^{k+1}} m dx. \tag{38}$$

where again the integral is approximated by a composite trapezium rule.

In the third stage the ice thickness H_i is recovered algebraically at the new time level using a discretised (midpoint rule) approximation of eq. (33), namely,

$$H_i^{k+1} = \frac{\theta^{k+1}(\mu_{i+1} - \mu_{i-1})}{(X_{i+1}^{k+1} - X_{i-1}^{k+1})}. \tag{39}$$

12

Note that from eq. (39) the discrete mass fractions

$$\frac{1}{\theta^k}(X_{i+1}^k - X_{i-1}^k)H_i^k \tag{40}$$

are conserved in time by this step.

5.1 The Discrete Diffusive Velocity at the Glacier Front

We now focus on the numerical approximation of the diffusive velocity at the front and relate it to the analysis in section 3 to show how the CMF approach gives good resolution of the waiting time behaviour at the snout. From (36) the approximation U_N to the diffusive velocity at the glacier front is given by

$$U_N = c \left(\frac{n}{2n+1}\right)^n \frac{(-H_{N-1})^{2n+1}}{(X_N - X_{N-1})^n}, \tag{41}$$

since $H_N = 0$. At first glance this bears little resemblance to eq. (13), where

$$u(b) \propto (b - x)^{(2n+1)\alpha - n} \tag{42}$$

But rewriting (41) using eq. (12), the analytic diffusive velocity can be written

$$u(b) \propto \frac{h^{2n+1}}{(b - x)^n}, \tag{43}$$

since $h \propto (b - x)^\alpha$, which has a similar form to eq. (41). When $\alpha > n/(2n + 2)$, both the numerator and denominator in eqs. (41) and (43) are small, but this is not the case if $\alpha = n/(2n + 2)$, as demonstrated in section 3.

The closer the nodes cluster at the glacier front, the more effective eq. (41) is at providing a good approximation to eq. (43). As the ice diffuses the gradient at the snout increases in modulus and the interval (X_{N-1}, X_N) decreases. The numerical scheme then well resolves the analytic behaviour of the diffusive velocity.

6 Testing the Model

As a first test consider the initial ice thickness profile from Section 3,

$$h = (b^2 - x^2)^\alpha \tag{44}$$

13

Physical Parameters	
$n = 3$	Flow-law exponent
$A = 10^{-16}(Pa)^{-3}a^{-1}$	Flow-law parameter
$g = 9.81ms^{-2}$	Acceleration of gravity
$\rho = 910kgm^{-3}$	Ice density
$c = -2Ag^n\rho^n/(n+2)$	Constant Parameter
$\gamma = 0.0005$	Scale of accumulation rate

Computational Data	
$N = 26$	Number of gridpoints
$\Delta x^0 = 0.02$	Initial grid spacing
$\Delta t = 0.05$	Time Step
T	Final Time

Table 1: Values of the physical parameters in the test problem and the computational data used in the test equations.

on an initial domain $x \in [0, b]$, where $x = 0$ is the fixed ice divide and the initial moving front is at $b = 1$. The accumulation term $m(x)$ is defined by the quadratic function

$$m(x) = \gamma \left(1 - \frac{x^2}{\beta} \right), \tag{45}$$

where β defines the equilibrium line and γ is a parameter which controls the scale of the source term. The function $m(x)$ is independent of time which allows a steady state solution with the boundary b_{ss} defined by

$$b_{ss} = \sqrt{3\beta}. \tag{46}$$

Using the parameters defined in Table 1 the numerical model and its behaviour is evaluated under different values of α.

Glacier in Advance: $\alpha = 3/7$, $\beta = \frac{1}{2}$, $T = 12000a$

Setting the equilibrium line $\beta = 1/2$ implies that the boundary at steady

state solution is greater than the initial boundary position and the overall motion is that of an advance. Figure 2a) demonstrates an overall increase in the amount of ice in the domain, along with movement of the front towards the steady state boundary $b_{ss} = \sqrt{1.5}$. With $\alpha = 3/7$ there is an initial diffusive velocity contributing to the movement of the boundary (see fig. 3a)).

Conversely, with $\alpha = 1$ the boundary initially retreats due to ablation until the ice thickness profile changes over time to satisfy the condition on the diffusive velocity at the boundary (see figs. 2 and 3b)).

Glacier in Retreat: $\alpha = 3/7$, $\beta = \frac{3}{10}$, $T = 6000a$

Setting the equilibrium line closer to the ice divide ($x = 0$), with $\beta = 3/10$ results in a steady state boundary to the left of the initial boundary and the front of the glacier retreats.

In Figure 2c) there is rapid initial retreat, where the boundary moves past the steady state location before stabilising and advancing back up to the steady state location. This is further evident in the nodal trajectory plot (fig. 3c)). Crucially the interior points also retreat in line with the boundary which means that the nodes avoid crossing paths, an important stability property for any moving mesh method.

Stationary Front: $\alpha = 1$, $\beta = 1$, $T = 1500a$

Selecting $\beta = 1$ in eq. (45) yields zero accumulation/ablation at the initial boundary. Under this condition the diffusive velocity becomes the sole contribution to the velocity at the boundary so the analysis in Section 3 holds. By setting $\alpha = 1$ the boundary is initially stationary.

It is clearly visible in Figure 2d) that the profile evolves towards an infinite gradient at the front so as to satisfy the finite diffusive velocity criteria in Section 3.1. Once this criteria is met the front begins to advance. Examination of the movement of the mesh nodes in Figure 3 shows that the interior nodes move towards the boundary until the condition on the boundary profile is satisfied and the boundary itself begins to move.

15
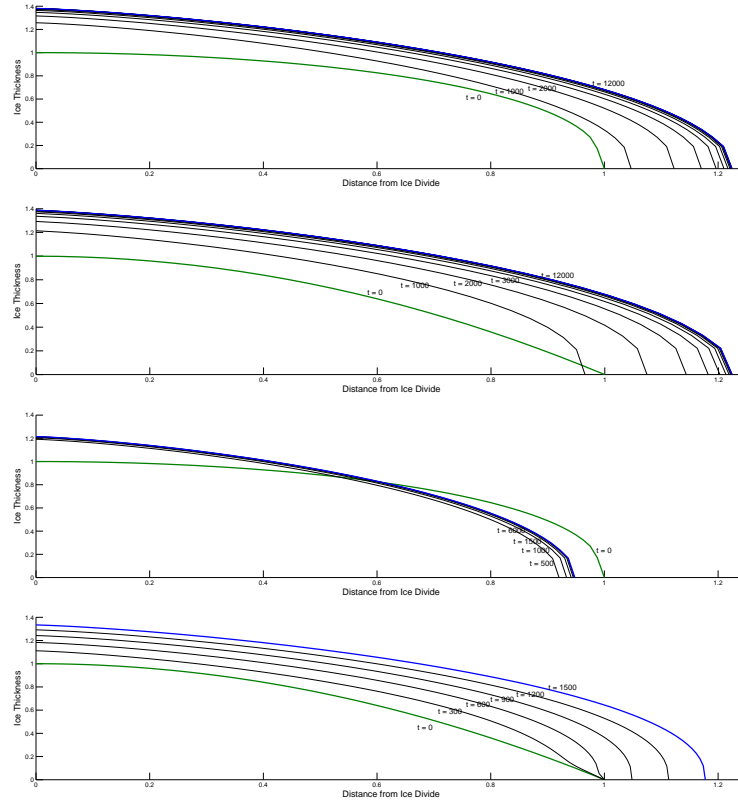
Figure 2: 1D test equations: Ice thickness over the domain evolving from the initial profile (green) to a final steady state profile (blue).

a) Advancing glacier; $\alpha = 3/7$, $\beta = \frac{1}{2}$,

b) Advancing Glacier; $\alpha = 1$,

c) Retreating Glacier; $\alpha = 3/7$, $\beta = \frac{3}{10}$ and

d) Initially Stationary Glacier; $\alpha = 1$, $\beta = 1$.

7 European Ice Sheet Modelling INiTiative

The European Ice Sheet Modelling INiTiative (EISMINT) experiments give a set of standard benchmark scenarios to test and compare numerical models
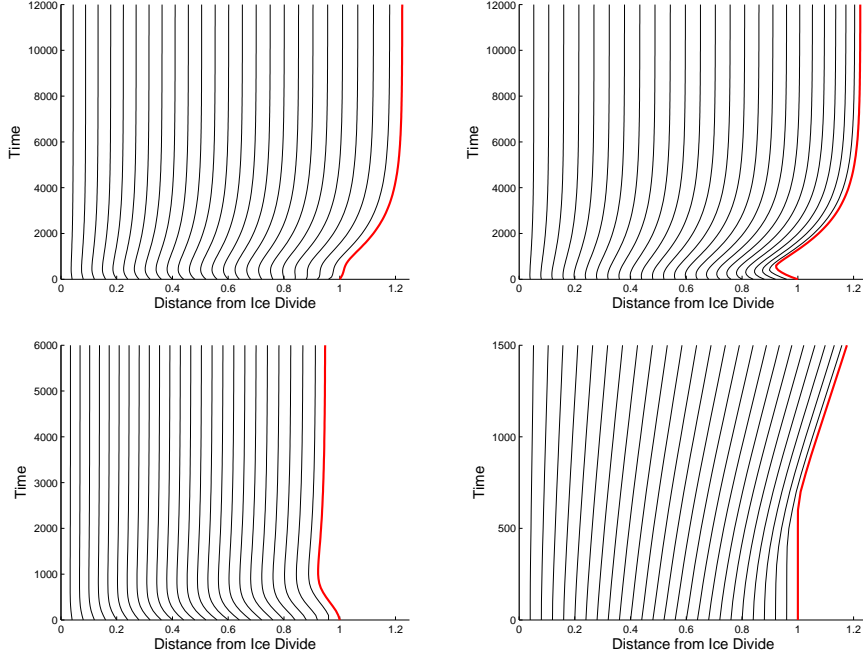
Figure 3: Evolution of the mesh nodes over time, including the boundary point (red) representing the glacier front.

a) Advancing glacier; $\alpha = 3/7$, $\beta = \frac{1}{2}$,

b) Advancing Glacier; $\alpha = 1$,

c) Retreating Glacier; $\alpha = 3/7$, $\beta = \frac{3}{10}$, and

d) Initially Stationary Glacier; $\alpha = 1$, $\beta = 1$.

of ice sheet behaviour. The initial paper [7] contains information about two scenarios; the first is a fixed margin experiment on a square domain which deals with calculating the ice discharge at the boundary, and the second is a radially symmetric situation with a moving boundary. Here the second experiment is replicated using the radially adjusted CMF method.

The experiment begins with a flat bed with zero ice present. The CMF method is dependent on preserving relative mass, which requires an initial mass to calculate: this is calculated using the ice thickness profile after one time-step

corresponding to the source term only, which is

$$m(x) = min\{0.5, \gamma(\beta - x)\}, \qquad (47)$$

The initial profile of ice thickness is therefore

$$h^0(x) = \Delta t \times min\{0.5, \gamma(\beta - x)\} \qquad (48)$$

with $x \in [0, 4.5 \times 10^5]$. The equilibrium line is located at $\beta = 4.5 \times 10^5 m$ in eq. (48) and the scale of the source term is given by $\gamma = 10^{-5}a^{-1}$. The source term is independent of time, so there exists a steady state solution in which the steady state boundary location is

$$b_{ss} = 579.81 km. \qquad (49)$$

Physical Parameters	
$n = 3$	Flow-law exponent
$A = 10^{-16}(Pa)^{-3}a^{-1}$	Flow-law parameter
$g = 9.81ms^{-2}$	Acceleration of gravity
$\rho = 910 kgm^{-3}$	Ice density
$m = min\{0.5, \gamma(\beta - x)\}$	Ice equivalent accumulation/ablation (source)
$\gamma = 10^{-2}ma^{-1}km^{-1}$	Slope of source function
$\beta = 450km$	Equilibrium line location
Computational Data	
$N = 16$	Number of gridpoints
$\Delta r^0 = 3^4 m$	Initial grid spacing
$\Delta t = 2a$	Time Step
$T = 3 \times 10^5 a$	Final Time

Table 2: Values used in the EISMINT scenario, including the physical parameters of the model and the computational data

The physical parameters are provided in table 2 along with the numerical data. For direct comparison with the results in [7] the model uses 16 grid points, initially spaced evenly. This allows for a time step of $2a$, up to a final time of $30000a$. The calculation takes less than five seconds to run on a standard desktop.

For such a radially symmetric problem the results of the one-dimensional flowline method may be presented as a circle which allows for ease of comparison with the two-dimensional data.

The numerical solutions to the experiment given in [7] are traditional fixed grid methods on evenly spaced grids. This means that they require some form of extrapolation or interpolation to find the boundary location as the boundary generally falls between two grid points. As a result the fixed grid methods on a regular two-dimensional rectangular grid, such as those presented, do not return a perfect circle due to the location of the grid points, as shown in fig. 4a). This is not an issue with radial flowline methods such as the one used here, which when rotated naturally give a circle (see fig. 4b)).

A better comparison is a direct comparison between flowline models. The moving mesh method is able to get significantly closer to the exact ice thickness profile than the equivalent fixed grid method in Figure 4c), especially near to the moving front. In Figure 4d) the diffusive velocity in steady state is similar in the two approaches, the main difference again arising at the boundary where the diffusive velocity can be explicitly calculated in the moving mesh approach. The fixed grid schemes require interpolation to calculate this value.

Expressing these results in table 3 shows that the CMF moving mesh solution is able to get much closer to the exact boundary position than the average fixed grid solution, whilst the thickness at the ice divide (where $x = 0$) is slightly higher than both the fixed grid and exact solutions.
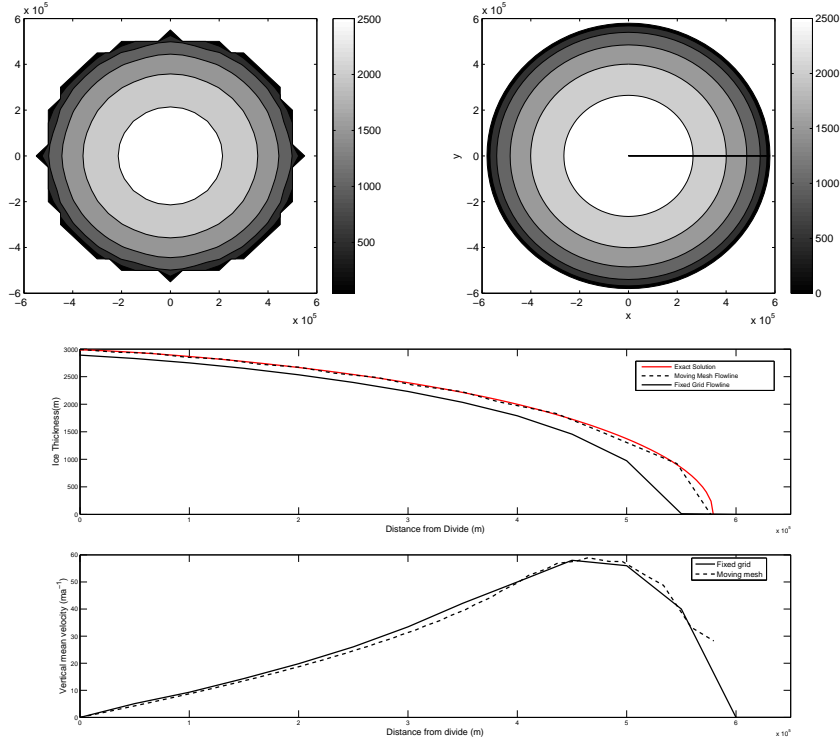
Figure 4: *a) 2D results from one of the fixed grid EISMINT experiments. b) Moving mesh flowline radial model converted to 2D. c) Ice thickness profile at steady state showing the exact (red), moving mesh (dash) and fixed grid (solid) solutions. d) Diffusive velocity at steady state showing moving mesh (dash) and fixed grid (solid) solutions.*

Experiment	Divide Thickness (m)	Boundary Position (km)
Avg EISMINT	2856.9	594.9
Moving Mesh	3005.3	576.9
Exact	2951.5	579.81

Table 3: Comparison between the average EISMINT experiment results, the moving mesh approach and the exact steady state solution.

8 Data Assimilation

While numerical models of ice sheets provide a good representation of the dynamical flow, uncertainties in the initial input data lead to errors as the simulation evolves. Moreover, observations describing the glacier system are incomplete and contain inaccuracies. Using data assimilation the two can be combined to gain a best representation of the true state of the ice sheet.

Here we employ a sequential assimilation approach, where the model is evolved from *a-priori* initial estimates until observations are available. The model prediction of the variables, denoted $\mathbf{z}^f$, is then corrected by a weighted difference between the observations $\mathbf{y}$ and the predicted observations $\mathbf{Cz}^f$ to obtain the *analysis* $\mathbf{z}^a$, the best representation. Mathematically this may be written as

$$\mathbf{z}^a = \mathbf{z}^f + \mathbf{K}(\mathbf{y} - \mathbf{Cz}^f), \tag{50}$$

where the matrix weight $\mathbf{K}$ is chosen to ensure that the scheme converges to the truth. A full list of variables is provided in Table 4.

By perfoming the assimilation the mass of the glacier is altered by using external information. Since the conservation principle depends on the total mass, a 'reset' of the constants μ_i is required in order for the method to proceed.

8.1 Experimental Design

In the test scenario there are no real observations available, so they have to be generated. To achieve this we assume that we know the exact initial domain, $x \in (0, 4.5 \times 10^5)$ with a corresponding ice thickness that satisfies the boundary conditions, and perform a 'truth run' using the output to generate 'observations'. Then the initial domain is altered to $x \in (0, 3 \times 10^5)$, and the ice thickness to 1.1 times that of the truth. The altered initial conditions are then evolved through time until the instant when observations of ice thickness taken from the exact

Value	Quantity
$\mathbf{z}$	Vector containing the unknown model variables
$\mathbf{y}$	Vector of observations
a	Superscript denoting the 'analysis', or best guess solution
f	Superscript denoting the prior solution, taken from the model
$\mathbf{C}$	Observation operator mapping observations to the model space
$\mathbf{K} = \mathbf{B}\mathbf{C}^T(\mathbf{C}\mathbf{B}\mathbf{C}^T + \mathbf{R})^{-1}$	Correction, or Gain Matrix
$\mathbf{B}$	Background error covariance matrix
$\mathbf{R}$	Observation error covariance matrix

Table 4: Data Assimilation variables

solution are applied and an assimilation step is performed. This procedure is known as a *twin experiment*. The state vector represents all the unknown values of the ice thickness, $\mathbf{z} = \{H_i\}_{i=1}^N$.

The observations are subject to random noise, $\mathbf{y} = \mathbf{C}\mathbf{z}^a + \mathbf{e}$, where $\mathbf{e} \sim N(0, \sigma_o^2)$ to simulate observation errors. Each observation is assumed independent of the others, so the covariance between them is zero and $\mathbf{R} = \sigma_o^2\mathbf{I}$. Since the observations are direct, linear interpolation is used to calculate the predicted observations for the matrix $\mathbf{C}$. We assume that the observations of ice thickness are within $\sqrt{30}m$ of the truth, i.e. $\sigma_o^2 = 30$.

The choice of the background error covariance matrix $\mathbf{B}$ is one of the most critical aspects of any data assimilation scheme, primarily representing the covariance relationship between the variables, although it also acts to spread information between variables. For fixed grid methods a typical correlation function between variables i and j to characterise the background errors is the
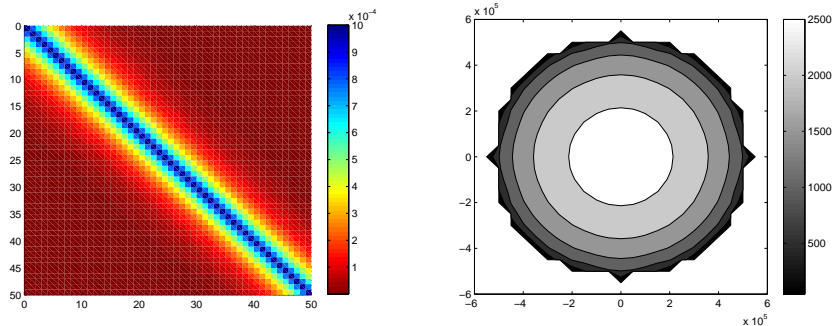
(a)
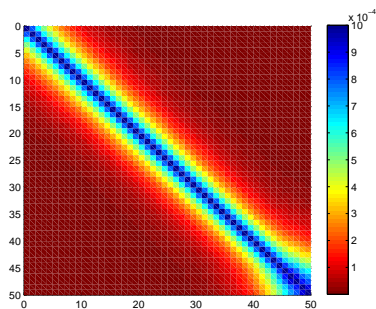
(b)

Figure 5: *Evolution of the B matrix; a) initial time, and b) after 40000 steps*

SOAR function [10], given by

$$b_{ij} = \sigma_b^2 \exp(-\Delta x/L)^{|i-j|}, \tag{51}$$

where Δx is the constant grid spacing, L a length scale and σ_b^2 a corresponding background error. This is modified for an irregular mesh method to

$$b_{ij} = \sigma_b^2 \exp(-|X_i - X_j|/L), \tag{52}$$

which allows for different spacing between points. We take $\sigma_b^2 = 30$, of the same order as the observations. This approach means that the B matrix needs to be recalculated at every assimilation step, which is computationally costly in practice. How this matrix evolves is demonstrated in Figure 5. At the initial time the mesh nodes are evenly distributed and the error covariances are evenly spread on the diagonal. Once the points have begun to move they spread out in the upper zone of the glacier and close up near the snout, reflected by a thinning

and thickening respectively of the diagonal strip.

This evolution of **B** is similar to the Kalman filter sequential approach, which forecasts the matrix as part of the scheme [11].

8.2 Observing the boundary

The primary characteristic of a moving mesh approach is that the domain is evolving over time. If the initial domain is in error then the evolution will also contain errors. Therefore we include observations of a moving physical feature to account for these errors, in this case the snout. To achieve this modification the mesh is treated as unknown and included in the state vector along with the ice thickness, so that

$$\mathbf{z} = \begin{pmatrix} \mathbf{X} \\ \mathbf{H} \end{pmatrix} \tag{53}$$

The **B** matrix then takes the form

$$\mathbf{B} = \begin{pmatrix} B_x & B_{xh} \\ (B_{xh})^T & B_h \end{pmatrix}, \tag{54}$$

where **X** and **H** are vectors representing the boundary and the ice thickness.

Both the B_h and the B_x entries use the modified SOAR function (eq. (52)) with a different σ_b^2. We set the cross covariance terms $B_{xh} = 0$. This means that if no observations of the boundary are available only the ice thickness variables will be updated and the mesh is unchanged.

8.3 Results

We examine two scenarios, depending on whether the boundary is observed or not. Figure 6 shows the results of an experiment for which no observations are available. The model is then combined with 8 randomly distributed observations of ice thickness at $t = 2000a$. Taking observations of the ice thickness does not correct the boundary position (fig. 6(a)) at the assimilation time, but as the simulation continues the corrected ice profile acts to pull the boundary back.

The ice thickness at the divide (fig. 6(b)) is corrected at the time of assimilation, along with the other ice thickness variables in the interior of the domain.
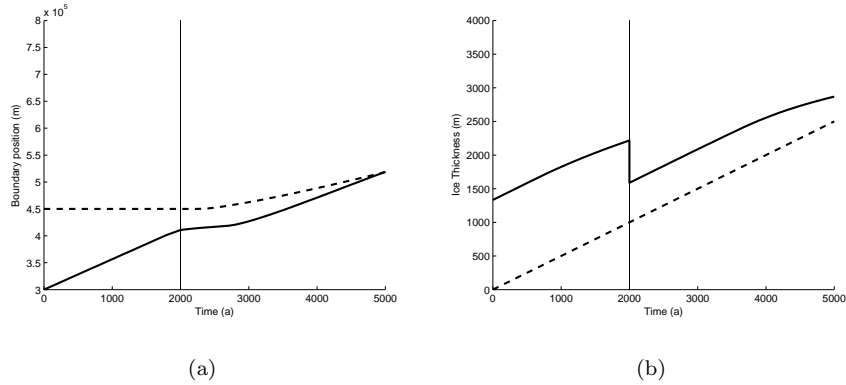
Figure 6: *Effect of data assimilation on two key features, (a) Position of the moving boundary, and (b) Ice thickness at the divide. Solid lines represent the prediction, dashed lines denote the truth.*

By also including observations of the true location of the boundary, the numerical representation of this point is pulled towards the true value (see fig. 7(a)). The interior mesh points are also updated through the form of (54). The ice thickness profile (fig. 7(b)) response is unaffected by the addition of a boundary observation. Fig. 7(c) shows the complete ice profile before (dash-dot) and after (dashed) observations of the truth (solid) are assimilated at $t = 2000$. We see from Fig. 7(d) that at the final time ($t = 5000$) the model that contained an assimilation step (dashed) is considerably closer to the truth (solid) than the model that contained no assimilation (dash-dot).

8.4 New Results

Taking two sets of observations shows the progression of the forecast towards the truth. Taking a large number of observations (in this case 30), spread as shown in Figure 8(c) and Figure 8(d), we expect the forecast to converge quickly to the truth. This is evident from the characteristic plot of both the boundary

(a)   (b)

(c)   (d)
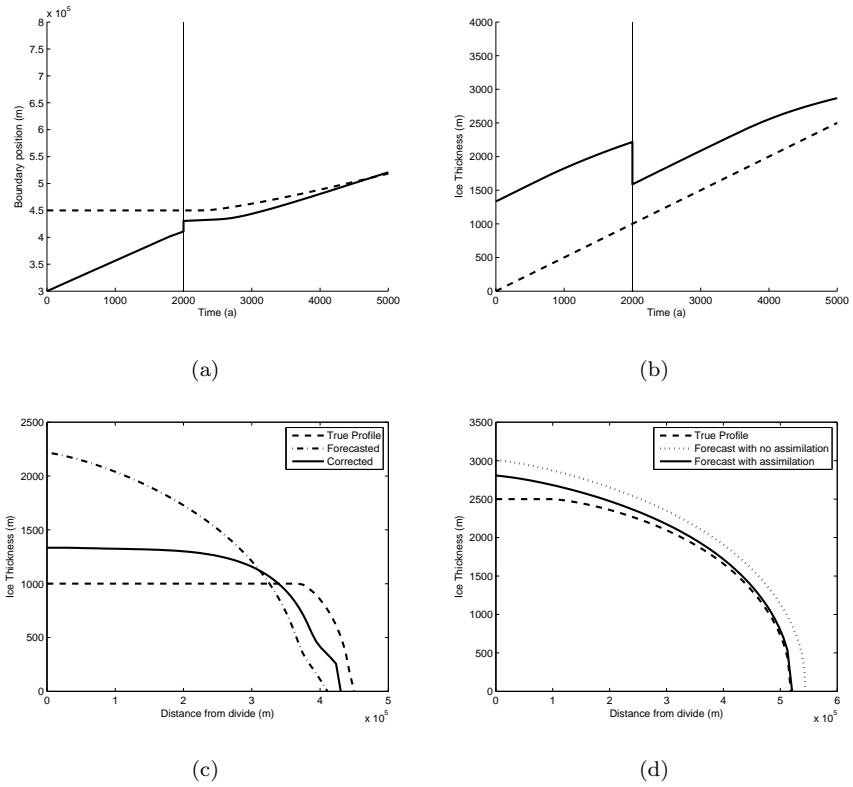
Figure 7: *The numerical domain is corrected as well as the ice thickness by augmenting the data assimilation acheme.*

(fig. 8(a)) and the ice divide (fig. 8(b)).

However in reality few observations are available. In that case we expect the forecast to still be corrected towards the truth when the observations are assimilated, but with less correction. Here we take six observations, spread as in Figure 9(c) and Figure 9(d). We see that the corrections in the boundary (fig. 9(a)) and the ice divide (fig. 9(b)) are smaller, and that the forecasted profile at the second assimilation time (fig. 9(d)) is further from the truth than fig. 8(d).

(a)   (b)

(c)   (d)
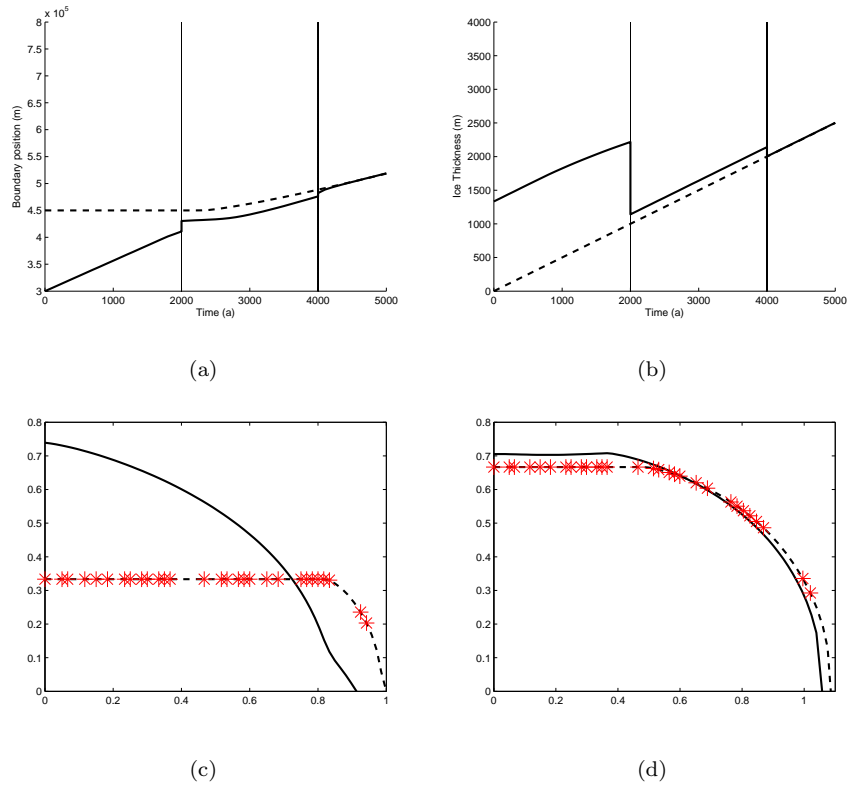
Figure 8: *Taking lots of observations causes the forecast to converge towards the truth at a fast rate*

9   Discussion

In this report, taking a standard one-dimensional glacier model under the shallow ice approximation we analysed the ice diffusion velocity, showing that it can exhibit a discontinuity at the snout (leading to a waiting time situation) and that a positive velocity corresponds to a particular asymptotic form of the ice thickness at the moving boundary. We also analysed the velocity of an arbitrary point of the domain under a conservation of mass fractions (CMF) description and showed that it can be written as a combination of the model velocity and an additional term depending on the ice equivalent accumulation rate.

We then introduced the CMF moving mesh method, based on the conservation
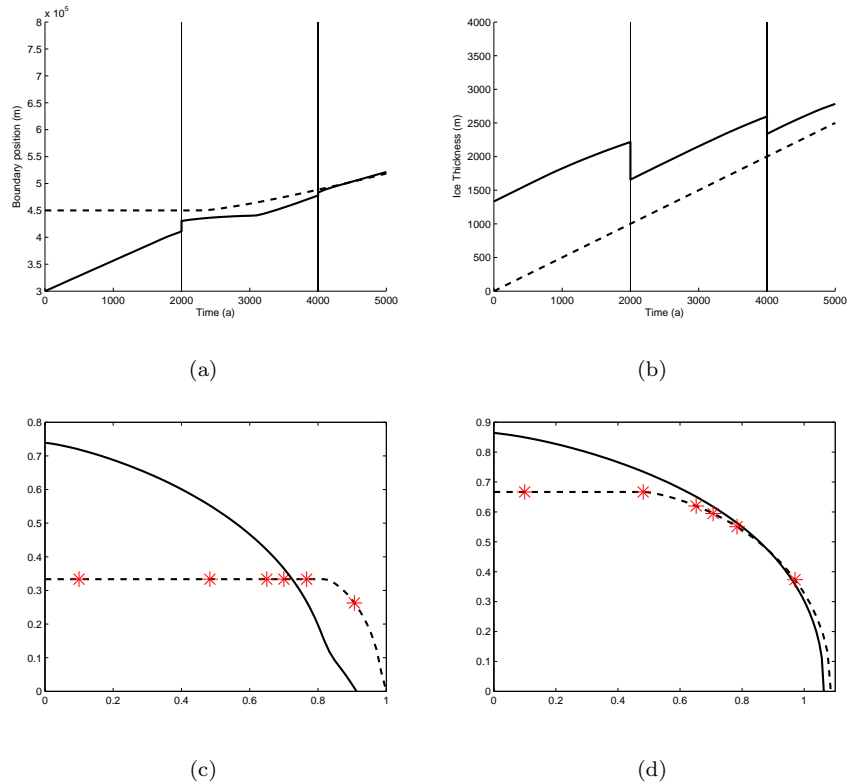
Figure 9: *When less observations are available the convergence to the truth is slower*

of mass fractions description, which qualitatively reproduces the main features of the boundary movement, including the waiting time phenomena mentioned above. By taking an expression that satisfies the boundary conditions and the local profile close to the boundary we were able to qualitatively simulate a waiting time situation for the snout velocity as the power law of the profile evolved towards a critical value from above. The CMF moving mesh method was then tested using the radially symmetric EISMINT scenario, with results closer to the exact solution than traditional fixed grid methods.

The concepts of data assimilation were then applied, showing that established methods can be extended to include the unknown mesh positions as part of the system in order to take advantage of observations of positional co-ordinates. We

noted that information is implicitly transfered through further iterations which avoids the need to determine the relationship between the mesh and the other model variables.

Whilst this paper uses a diffusive velocity given by the shallow ice equations the moving mesh approach is independent of the form of the velocity and could be used as a solver for mass conservation alongside the more complex Navier-Stokes descriptions of diffusive flow.

An implementation of the CMF approach in modelling the grounding line can be found in [4].

References

[1] M. J. Baines, M. E. Hubbard, and P. K. Jimack. A moving mesh finite element algorithm for the adaptive solution of Time-Dependent Partial Differential Equations with Moving Boundaries. *App. Num. Math.*, 54: 450–469, 2005.

[2] M. J. Baines, M. E. Hubbard, and P. K. Jimack. Velocity-based moving mesh methods for nonlinear partial differential equations. *CiCP*, 10:509–576, 2011.

[3] W. Cao, W. Huang, and R. D. Russell. Approaches for generating moving adaptive meshes: location versus velocity. *Applied Numerical Mathematics*, 47:121–138, 2003.

[4] J. Dodd. A Moving Mesh Approach to Modelling the Grounding Line in Glaciology. M.Sc.Thesis, Department of Mathematics and Statistics, University of Reading, UK, 2013.

[5] J. W. Glen. The Creep of Polycrystalline Ice. *Proc. R. Soc. Lond. A* 1955, vol. 228 pp. 519-538.

[6] K. Hutter. *Theoretical Glaciology*. Springer, 1983.

[7] P. Huybrechts and T. Payne. The EISMINT benchmarks for testing ice-sheet models. *Annals of Glaciology*, 23, pp 1-12, 1996.

[8] D. Partridge and M. J. Baines. A moving mesh approach to an ice sheet model. *Computers and Fluids*, 46, 2011.

[9] A. Vieli and A. J. Payne. Assessing the ability of numerical ice sheet models to simulate grounding line migration. *J. Geophys. Res*, Volume 110, Issue F1, 2005.

[10] C. D. Rodgers, *Inverse methods for atmospheric sounding*, World Scientific Publishing Co. Pte. Ltd, 2000.

[11] R. E. Kalman, A new approach to linear filtering and prediction problems, *ASME Journal of basic engineering*, Volume 82 ,1960.